

Probing $5f$ -state configurations in URu_2Si_2 with U L_{III} -edge resonant x-ray emission spectroscopy

C. H. Booth,¹ S. A. Medling,^{1,2} J. G. Tobin,^{3,*} R. E. Baumbach,^{4,†}
E. D. Bauer,⁴ D. Sokaras,⁵ D. Nordlund,⁵ and T.-C. Weng^{5,‡}

¹*Chemical Sciences Division, Lawrence Berkeley National Laboratory, Berkeley, California 94720, USA*

²*Electronic Materials Engineering, Australian National University, Canberra, 2602, Australia*

³*Materials Science Division, Lawrence Livermore National Laboratory, Livermore, California 94550, USA*

⁴*Materials Physics and Applications Division, Los Alamos National Laboratory, Los Alamos, New Mexico 87545, USA*

⁵*Stanford Synchrotron Radiation Lightsource, SLAC National Accelerator Laboratory, Menlo Park, California 94025, USA*

(Dated: To be published in Physical Review B)

Resonant x-ray emission spectroscopy (RXES) was employed at the U L_{III} absorption edge and the $L_{\alpha 1}$ emission line to explore the $5f$ occupancy, n_f , and the degree of $5f$ orbital delocalization in the hidden order compound URu_2Si_2 . By comparing to suitable reference materials such as UF_4 , UCd_{11} , and $\alpha\text{-U}$, we conclude that the $5f$ orbital in URu_2Si_2 is at least partially delocalized with $n_f = 2.87 \pm 0.08$, and does not change with temperature down to 10 K within the estimated error. These results place further constraints on theoretical explanations of the hidden order, especially those requiring a localized f^2 ground state.

I. INTRODUCTION

It has often been said that the most interesting physics occurs when competing interactions are of nearly the same magnitude. Such a situation is surely occurring at URu_2Si_2 's so-called "hidden-order transition" (HO), which is a second-order phase transition at 17.5 K with a large ($0.2R \log 2$, where R is the universal gas constant) change in entropy that has nevertheless so far defied attempts to identify its order parameter.¹⁻³ Despite this conundrum being identified in the late 1980s and the fact that the HO transition presages a 1.5 K superconducting transition, the identification of the HO order parameter remains elusive, although progress has been steady since that time and URu_2Si_2 remains an important research subject today.⁴ Much of the recent work has been spurred by new innovative theories and concomitant improvements to experiments made possible both by better capabilities and single crystals. An important dividing line between the different theories of HO focuses on the nature of the $5f$ orbital, specifically, the $5f$ -orbital occupancy, n_f , and the degree of itinerancy.⁵ Various spectroscopic measurements of these quantities have been performed, without a clear consensus. In an effort to clarify the role of n_f and $5f$ localization, the work described below provides measures of both n_f and the degree of $5f$ -orbital localization using resonant x-ray emission spectroscopy (RXES) at the U L_{III} absorption edge and U $L_{\alpha 1}$ emission line.

The history of theoretical work describing HO in URu_2Si_2 is vast.^{5,6} For this short introduction, we only focus on some specific aspects. Some of the earliest theories relied on the existence of a localized f^2 , $J = 4$ configuration to generate certain crystalline electric field (CEF) symmetries. Although CEF signatures have never been definitively observed, some recent innovative work once more depends on their existence,⁷⁻¹² while other work focuses on an itinerant model of the $5f$ electrons

starting from a partially occupied f^3 orbital.^{13,14} The DFT+DMFT calculations may form an interesting intermediate starting point, assigning the CEF states to the $j = 5/2$ shell and itinerant states to the $j = 7/2$ shell.^{12,15,16}

Experimental investigations are similarly divided in their interpretations. For instance, neutron scattering results show that a spin excitation gap can explain the change in the specific heat at 17.5 K, but is not consistent with localized physics.¹⁷ Likewise, recent NMR experiments looking at Knight shift anomalies are modeled such that the HO emerges directly from a Kondo liquid state, and is thus not associated with localized moments.¹⁸ In addition, neutron scattering has not definitively observed any CEF states.¹⁹ On the other hand, thermal conductivity measurements indicate a transition from itinerant to localized behavior in the HO state.²⁰ Other indications of at least a partially localized f^2 configuration exist, together with indications of dynamical CEF excitations.²¹ In addition, recent experiments highlight the possible importance of symmetry changes. For instance, cyclotron resonance measurements show an anomalous splitting of the sharpest resonance line under in-plane magnetic field rotation, likely caused by the fourfold rotation symmetry of the tetragonal lattice being broken by domain formation, and consistent with the suggestion that there is a nematic Fermi liquid state (where itinerant electrons have unidirectional correlations).²² This result is supported by high-resolution synchrotron x-ray diffraction results.²³ Other measurements indicating possible tetragonal symmetry breaking in the HO state include a recent measurement of a long-lived low energy excited-state chirality density wave with A_{2g} symmetry from Raman spectroscopy,¹⁵ consistent with inelastic neutron scattering anisotropy results.²⁴ However, this conclusion remains controversial; for instance, recent inelastic neutron results show no indications of reduced spatial symmetry,¹⁹ raising the possibility that such sym-

metry breaking only happens in the smaller samples less suitable for neutron experiments. Moreover, comparisons of the DC magnetic susceptibility $\chi(T)$ of a system thought to possess a tetravalent singlet crystal field ground state similar to that proposed for URu₂Si₂ show little resemblance.²⁵

Ultimately, determining specific and quantitative details about n_f and $5f$ itinerancy require spectroscopic measurements. Photoemission (both angle-integrated and angle-resolved) results generally favor delocalized $5f$ states and paint a very interesting picture of the details of the Fermi surface.²⁶ In particular, the larger features in the band structure and Fermi surface of URu₂Si₂ measured by soft x-ray photoemission in the paramagnetic (PM) state above the HO transition are well explained by treating all of the U $5f$ electrons as itinerant with $n_f \approx 2.6$.²⁷ Furthermore, these photoemission experiments indicate a large electron-like sheet around the Γ point, with smaller hole-like structures forming around the Z point.²⁷ It is important to note, however, that not all features in photoemission are well described by LDA calculations. For instance, some indications of an f^2 contribution have also been observed in core-level and valence-band photoemission that are otherwise indicating a close to f^3 ground state.²⁸ In addition, changes in the HO phase include a Fermi surface restructuring²⁹ involving folding along $Q_0 = (0, 0, 1)$ and gapping along the $(1, 1, 0)$ directions.³⁰

Although the photoemission experiments have provided valuable insight into the electronic structure of URu₂Si₂, they are limited by surface-sensitivity concerns and by having to compare to calculations in order to determine a value for n_f .²⁶ One technique that is less sensitive to the exact electronic details is electron energy-loss spectroscopy (EELS). EELS experiments suggest that URu₂Si₂ has $5f$ states which are more localized than α -U (even at room temperature), but still not completely localized, with a $5f$ electron count $n_f = 2.7 \pm 0.1$ suggesting a mixed valence ground state and/or some $5f$ -electron itinerancy.³¹ However, other interpretations question the usefulness of EELS in this respect in uranium compounds,³² implying that further support is needed. In addition, the degree of surface sensitivity in this electron spectroscopy technique remains a concern.

Photon-in/photon-out techniques are inherently less surface sensitive, although a soft x-ray experiment of this type is much more surface sensitive than a hard x-ray experiment. A recent O edge x-ray absorption spectroscopy (XAS) measurement, combined with resonant inelastic scattering (RIXS) and including polarization dependence,²¹ concludes that only features derived from an f^2 ($J = 4$) ground state are clearly observed; however, it is noted that f^3 features could be obscured by itinerancy, which has not yet been considered with experimental model compounds. The measurements observed only short-lived ($\Gamma \gtrsim 0.1$ eV) CEF modes, and found that these could account for most or all of the CEF excitation intensity expected in an f^2 multiplet picture. Taken to-

gether, although features associated with the f^2 atomic multiplet ground state ($J = 4$) are clearly observed, the total $5f$ occupancy is not determined by these data. Likewise, the large inverse lifetime of CEF excitations (0.1 eV $\gg 1/k_B T$) implies that electronic itinerancy cannot be dismissed as a perturbative factor.

An independent, truly bulk-sensitive method for determining n_f is clearly highly desirable. U L_{III} RXES should be able to provide such an independent measure of n_f , while potentially also drawing a distinction between a Kondo-like, mixed valence mechanism and a $5f$ -band interpretation, but there are challenges. The technique involves measuring the U $L_{\alpha 1}$ x-ray emission as a function of energy using a high resolution spectrometer while sweeping the incident x-ray energy just above and below the U L_{III} absorption edge. The average depth of an emitting photon above the photoelectron threshold energy is about $1.9 \mu\text{m}$,³³ and is deeper below the threshold where much of the data and analysis occur. The resulting spectral broadening is dominated by the final-state $3d_{5/2}$ core hole lifetime, and hence provides a higher resolution measure of the unoccupied $6d$ states near the Fermi energy, E_F , than a conventional L_{III} -edge x-ray absorption near-edge structure (XANES) experiment, which is dominated by the shorter-lived $2p_{3/2}$ core hole. Either RXES or XANES experiments can potentially differentiate between a localized mixed valence state and a simple partially-filled band if the Coulomb interaction between the core hole and the f -electrons is strong enough to break the mixed valence state into its configurations with different numbers of f -electrons.³⁴ In a typical Yb intermetallic, for instance, the Coulomb interaction splits the $4f$ state into f^{13} and f^{14} configurations, which screen the outgoing photoelectron differently, resulting in two distinct features in the $2p$ - $5d$ absorption spectrum that are about 10 eV apart.^{35,36} Such splitting in uranium should be approximately the same as observed between valence states, which is on the order of ≈ 5 eV based on studies of various oxide materials.^{37,38} On the other hand, if the $5f$ -electrons are more delocalized, an overall shift of the main absorption feature may occur instead of split features, since the Coulomb interaction may then be of insufficient strength. These complications need to be considered when analyzing either XANES or RXES U L_{III} spectra.

A further complication can occur in the presence of strong ligand fields, where splitting can occur between t_{2g} and e_g states in the d manifold. If this splitting approaches the ≈ 5 eV expected between valence states in U, then deconvolving ligand-field splitting and intermediate valence effects may not be possible. However, one expects that such ligand-field splitting should be relatively small in an intermetallic compound like URu₂Si₂ compared to a more π bonded system like UO₂.

In consideration of these effects, the rest of this paper is organized as follows: After a description of the Experimental Details, RXES results from UO₂ and UF₄ will be compared to those from UCd₁₁ as examples of standard

materials exhibiting various degrees of localized $5f$ behavior, ligand-field splitting in the d manifold, and both f^2 and f^3 spectroscopic features. Subsequently, results from URu₂Si₂ will be presented and considered in light of potential localized/delocalized behavior and ligand-field splitting.

II. EXPERIMENTAL DETAILS AND METHODS

A single crystal of URu₂Si₂ was grown by the Czochralski technique and subsequently electro-refined. Two samples were cleaved from this crystal. Such cleaves routinely yielded high-purity crystals with residual resistivity ratios $\text{RRR} = \rho(300 \text{ K})/\rho(0 \text{ K})$ between 200-400, where $\rho(0)$ was obtained from a power law fit to the electrical resistivity of the form $\rho(T) = \rho_0 + AT^n$ at low temperatures. The RRRs for these specific cleaved samples for the RXES experiments were not measured. While each sample was chosen for the spectroscopic measurements to have an optically flat portion for easy sample alignment, after preliminary measurements, a single sample was chosen for the measurements presented here.

RXES data were collected during two experimental runs about one year apart at the Stanford Synchrotron Radiation Lightsource (SSRL) wiggler beamline 6-2 using a LN₂-cooled Si (311) double monochromator calibrated so that the inflection point of the Zr K -edge absorption from a Zr reference foil was at 17998.0 eV. The emission was measured using a seven-crystal Ge(777) Johann-type x-ray emission spectrometer,³⁹ at an emission energy, E_e , of approximately 13.6 keV, corresponding to the U $L_{\alpha 1}$ emission. The emission spectrometer energy was calibrated using the direct scatter from a polycarbonate film with the incident energy, E_i , set to the first inflection point of the absorption at the Au L_2 edge from a Au reference foil (13734 eV). The total emission energy resolution (including the incident beam) was measured to be 1.4 eV.

At these energies, the information depth of the x-rays is greater than 1.9 μm ,³³ so these measurements are truly bulk sensitive. The sample was visibly shiny for both experimental runs, and no particular care was taken to avoid surface oxidation.

The sample of URu₂Si₂ was placed with its surface normal at a 45° angle with respect to the incoming beam. Data were collected at 10, 15, 20, 22, 50, 90, and 300 K using a LHe-flow cryostat. Owing to the relative thickness of the sample, a self-absorption correction was applied,⁴⁰ as well as a dead-time correction.

The RXES emission intensity data, I_e , are fitted with previously published methods⁴⁰, using the Kramers-Heisenberg equation of the form:

$$I_e(E_i, E_t) = \int d\epsilon \eta(\epsilon) \frac{A}{(E_{gi} - \epsilon + E_i)^2 + \Gamma_i^2/4} \times \frac{\Gamma_f/(2\pi)}{(E_{if} - \epsilon + E_t)^2 + \Gamma_f^2/4}. \quad (1)$$

Here, $E_t = E_i - E_e$ is the energy transferred to the sample in the final state, E_{gi} is an energy scale corresponding to the energy difference between the ground and intermediate state, E_{if} is another energy scale corresponding to the energy difference between the intermediate and the final state, Γ_i is the lineshape broadening due to the finite lifetime of the intermediate state core hole (here, the $2p_{3/2}$ core hole), and Γ_f is similarly due to the finite lifetime of the final state core hole (here, the $3d_{5/2}$ core hole). For a more complete discussion of Eq. 1, please see Refs. 40,41. In the fits described below, we have chosen to fix Γ_i and Γ_f to their nominal values⁴² of 8.104 eV and 3.874 eV, respectively, although allowing these parameters to float generally gives results close to these values and does not significantly change the results described below. In these experiments, the ground state includes $2p_{3/2}3d_{5/2}6\bar{d}$ electrons, the intermediate state has $2\bar{p}_{3/2}3d_{5/2}6d$ electrons, and the final state has $2p_{3/2}3\bar{d}_{5/2}6d$ electrons, where the bar indicate a hole. Eq. 1 is simplified assuming the transition matrix elements T_1 and T_2 in $A \propto \langle f|T_2|i\rangle^2 \langle i|T_1|g\rangle^2$ have no off-diagonal terms.

The most important aspect of the fitting is the choice of the local unoccupied density of states $\eta(\epsilon)$. As described in Ref. 40, we allow for three different possible $5f$ configurations within the ground state:

$$|f\rangle = c_2|f^2\rangle + c_3|f^3\rangle + c_4|f^4\rangle, \quad (2)$$

where c_i^2 give the probability of finding the system in any one configuration f^i . The presence of the core hole in both the intermediate and the final state will interact differently with each configuration, and if this Coulomb interaction is large enough, these states will split.³⁴ This splitting is reflected in the empty $6d$ states. As before,^{32,40,43} we parametrize $\eta(\epsilon)$ with a combination of a so-called ‘‘peak’’ Gaussian (each constrained to the same width σ_p) to represent the excitations into the comparatively discrete empty $6d$ states and a broadened step function (same σ_p and the height of the peak Gaussian defined relative to the step height defined to be the p/s ratio) to represent the continuum of unoccupied states. Each potential configuration is then represented by this combination of a Gaussian and the step function. More details with regard to the specific fits are provided below.

III. RESULTS

A. Calculations and measurements on UF₄ and UO₂

In order to consider the $5f$ -orbital occupancy and localization features of URu₂Si₂, comparisons to standard materials are essential. In this case, the standard materials would ideally be ones with strongly localized $5f$ -orbitals in the f^2 (tetravalent uranium) and f^3 (trivalent uranium) configurations. From our previous work,^{43,44}

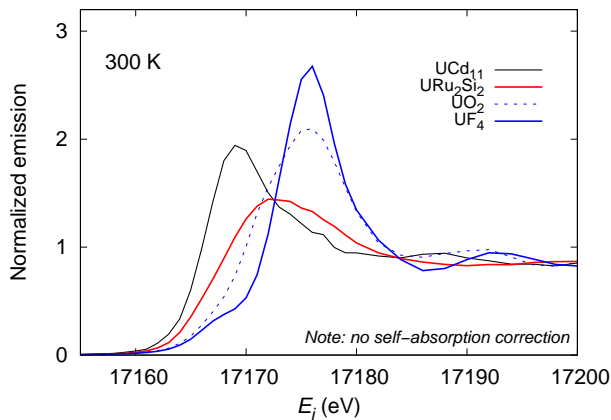


FIG. 1: PFY measurements of UCd_{11} (black), URu_2Si_2 (red), UO_2 (blue dotted), and UF_4 (blue) each collected at 300 K. Note that a self-absorption correction is not applied to these data to better place them on the same scale and to accentuate the feature in the UF_4 spectrum on the lower shoulder of the main edge near 17167 eV.

we identified UCd_{11} as possessing strongly localized $5f$ electrons and $n_f = 2.86 \pm 0.08$, which is sufficiently close to f^3 to act as a good standard.⁴³ Unfortunately, although there are only a few intermetallics thought to possess a localized f^2 configuration, we have not succeeded in obtaining data on sufficiently localized intermetallic samples of this type. Instead, we can rely on data from UF_4 as an unquestionably localized f^2 material.³²

High-resolution partial fluorescence yield (PFY) data are shown in Fig. 1 for all measured samples. As indicated, the self-absorption correction was not applied to the data in this figure as a convenient way to accentuate the clear shoulder peak at about 17167 eV in the UF_4 spectrum. As is clearly seen, the so-called “white line” (WL) peak in UCd_{11} is shifted by 7-8 eV relative to that of UF_4 . The UO_2 and URu_2Si_2 spectra are clearly broader, and the WL peak energy of URu_2Si_2 is between that of UCd_{11} and UF_4 .

There are two features of the standards spectra that can be elucidated with cluster calculations, namely the broadening of the UO_2 spectrum and the shoulder feature in the UF_4 spectrum. Starting with the UO_2 spectrum, we note that in previous work, we have used UO_2 as a localized f^2 standard, but have recently found it to be a problematic example. UO_2 is considered to be a correlated-electron material and a Mott-Hubbard insulator,^{45,46} and as such, it may have a $5f$ occupancy that deviates from two and even have some direct $5f$ -band involvement at the Fermi energy. More importantly, the ordered cubic symmetry and octahedral coordination of the U-O nearest neighbors generates a substantial crystal field splitting of the unoccupied d states, a situation that is reduced in the more complex monoclinic structure of UF_4 .

This situation is illustrated by the results in Fig. 2

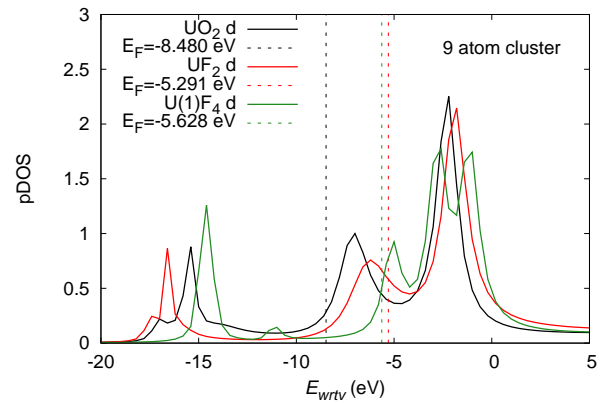


FIG. 2: Local density of states from FEFF LDA approximation for a 9 atom cluster of UO_2 (black), UF_2 (based on the UO_2 structure, red), and the U(1) site in UF_4 (green). E_F for each calculation is shown as a vertical dotted line.

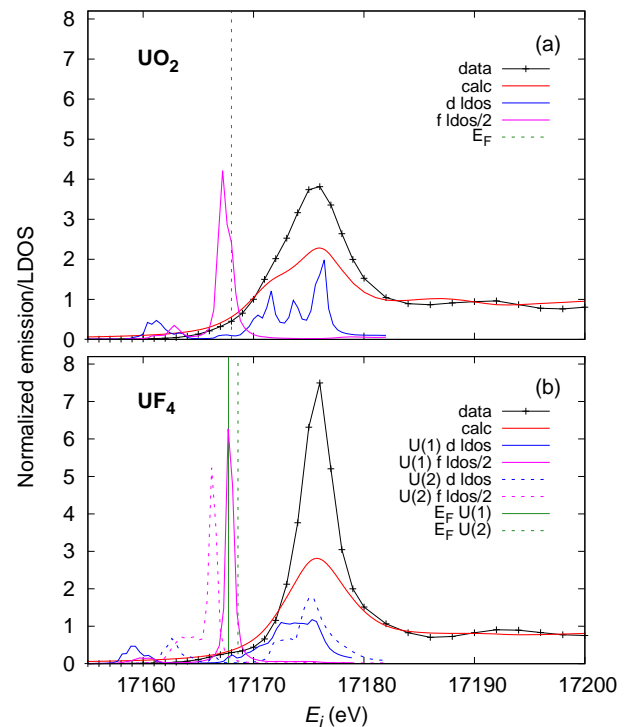


FIG. 3: PFY data shown together with a narrowed XANES and the corresponding local density of states calculations from FEFF LDA approximation for a 9 atom cluster of (a) UO_2 and (b) UF_4 . Calculations are shifted by (a) 17177.0 eV and (b) 17173.9 eV relative to the vacuum energy.

of a 9 atom cluster calculation of the local d density of states using FEFF 9.6.4.⁴⁷ In this simplified calculation, we use default FEFF behavior, which includes not allowing for charge transfer out of the $5f$ orbitals. Three curves are shown. In each calculation, only the first shell of 8 oxygen or fluorine atoms are included along with

the absorbing uranium atom. The small cluster size was chosen to emphasize the short-range, ligand-field nature of the e_g and t_{2g} features. The UO_2 calculation uses the nominal fluorite structure⁴⁸ and the UF_4 calculation uses the nominal monoclinic structure.⁴⁹ To demonstrate the role of the fluorine atom as opposed to the difference in crystal structure, we also show a calculation on “ UF_2 ”, which is really the same calculation on the same structure as the UO_2 calculation, except all the oxygen atoms are replaced by fluorine.

A number of features are important to discuss with regard to how UO_2 and/or UF_4 make a suitable localized f^2 U L_{III} absorption standard. In all three calculations, there is an e_g state, moving from about -7 eV in UO_2 (with respect to the vacuum energy) to about -5 eV in UF_4 . The t_{2g} state is at a somewhat higher energy, all centered at about -2 eV, with the UF_4 calculation showing a ≈ 1.5 eV split. These calculations therefore demonstrate that the e_g/t_{2g} ligand field splitting is reduced from UO_2 as one moves to the more ionic/less covalent “ UF_2 ” compound and then further to the less symmetric UF_4 compound.

These differences can be seen in the resulting absorption calculations shown in Fig. 3, where we now show the calculations on the “real” UO_2 and UF_4 structures for comparison to actual data (which now includes the self-absorption correction). These calculations include all atoms within a 6.58 Å radius of the central absorption uranium, and take into account the two uranium sites in the UF_4 structure, as noted. The spectra are calculated as L_{III} -edge absorption spectra but narrowed by 4.2 eV (FWHM) to account for the limiting factor of the $3d_{5/2}$ core hole instead of the $2p_{3/2}$ core hole. In addition, charge transfer out of the $5f$ orbital is allowed (the UNFREEZE card is employed). In order to obviate the ≈ 0.05 % threshold energy errors in FEFF calculations, the calculations are shifted by the amounts indicated in the figure caption so that the WL energies agree with the data.

While one can clearly see the effect of the larger ligand field splitting in the UO_2 calculation and the data compared to those of UF_4 , it is clear that FEFF overestimates the size of this splitting in each case. This overestimate is particularly clear in the UF_4 calculation, which shows more weight than the experimental data near 17170 eV, in a region of the spectrum between the shoulder feature at 17167 eV and the main edge.

A fascinating feature of the calculation on UF_4 is the difference in E_F between the U(1) and U(2) sites. While bearing in mind that potential errors exist in the determination of E_F , the FEFF calculations show a distinct energy shift in the $5f$ density of states between the U(1) site and the U(2) site (there are double the number of U(2) sites in the UF_4 lattice structure). This shift places the Fermi level within the U(1) density of states, a situation that also occurs, although to a lesser degree, in the UO_2 calculation. The significance of this shift is that, according to these calculations, unoccupied spectral weight

occurs in the $5f$ band at or just above E_F , which is accessible to the photoelectron excited from the $2p_{3/2}$ shell either from a dipole excitation through hybridization with the d orbitals or directly through a quadrupole transition, as previously considered for UO_2 .⁵⁰ The position and size of this feature are in very good agreement with the FEFF calculation as shown, which does not include any quadrupole term in the excitation. Including such a term vastly over estimates the size of the feature, possibly due to the $5f$ weight at the Fermi energy. We therefore tentatively conclude that this feature is primarily due to f/d hybridization, consistent with several photoemission studies.²⁶

An interesting issue in these calculations is that the calculated E_F is about 3 eV lower in UO_2 than the other calculations. This difference exists in both the small cluster and the 6.58 Å radius calculations. Fermi energy shifts are a common problem in FEFF, but this particular shift may be a reflection of the correlated electron nature of UO_2 , a quality that FEFF cannot capture. E_F directly affects the photoelectron threshold energy, yet no shift is observed in the experimental data in the white-line position between UO_2 and UF_4 (Fig. 1). It should therefore be noted that the absorption calculation in Fig. 1(a) is with respect to E_F , rather than with respect to vacuum, in order to make a direct comparison between the calculations and between the calculations and experiment.

The implication of these data and calculations for the purposes of this study is that the ligand field splitting is a complicating factor in the UO_2 spectra when using such spectra to model f^2 behavior in metals where such splitting will be reduced. In contrast, UF_4 appears to be a much better, and less covalent, model for such comparisons. In fact, the ligand field splitting is even less clear in larger cluster calculations of UF_4 , creating an even sharper absorption white line. Therefore, the combination of more ionic bonding (through the replacement of oxygen with fluorine) and reduced symmetry (which further reduces the ligand field splitting) allows UF_4 to be used as a close-to-ideal localized f^2 absorption standard material.

B. Comparisons between standard materials and URu_2Si_2

RXES data at 300 K for the standard materials and URu_2Si_2 are shown in Fig. 4. We begin with a discussion of the features in the various data sets before describing the fit results below. First, comparing the different standard materials, differences are most easily observed and interpreted well below the L_{III} threshold energy. In this method of presenting the data, the data below threshold are toward the bottom of the plot and the features in such data are at a relatively fixed E_t . It is clear from these data that the UF_4 and UCd_{11} spectra are each relatively sharp in character, while separated by about 7 eV, consistent with, but even larger than, the ≈ 5 eV shift ex-

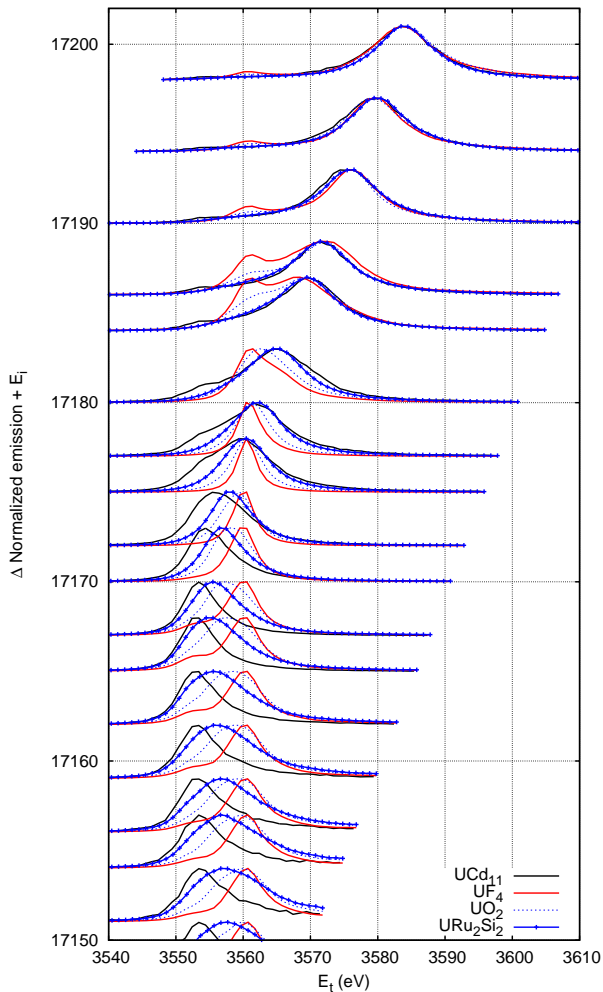


FIG. 4: Stacking plot for the UCd_{11} , UO_2 , and UF_4 standards together with data from URu_2Si_2 , all collected at 300 K. Each constant- E_i scan is normalized to maximum emission flux so that data near resonance (very high flux) can be placed on the same scale as, and thus more easily compared with, data well below resonance. Note that this normalization scheme obscures the fact that the unnormalized emission flux below threshold (~ 17170 eV for all these samples) is significantly lower than the emission flux above threshold.

pected for a $1 e^-$ difference in their $5f$ shells (Sec. I). The effect of the ligand field splitting in UO_2 is pronounced in these data, with a significantly broader spectrum below threshold. In addition to this broadening, there is a small positional shift of the XES peak (more easily observed at low E_i , which is also rationalized by the ligand field splitting).

The URu_2Si_2 data fall between the limits defined by the UCd_{11} and the UF_4 data, with a significant amount of spectral weight at both extremes. The lower-energy weight is even more clearly observed as it becomes resonantly enhanced near $E_i \approx 17166$ eV. It is interesting to compare these URu_2Si_2 results to those from UO_2 , since the energy shift toward UCd_{11} is substantially larger and

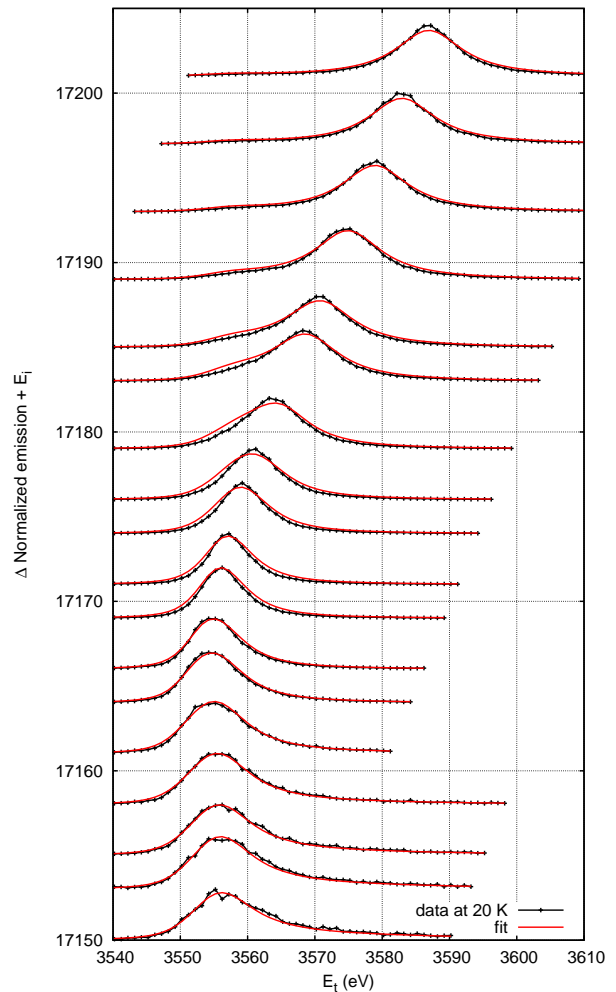


FIG. 5: RXES data and fit using model 2 at 20 K for URu_2Si_2 .

the spectra are significantly broader compared to those from UO_2 . Since no large ligand field splitting is expected in the d manifold in URu_2Si_2 , it seems very unlikely that it could be larger in URu_2Si_2 than in UO_2 .

Given the magnitude of the negative energy shift of the URu_2Si_2 spectra relative to UF_4 (and UO_2) is too large to be explained by ligand field splitting, the sign of this shift is significant: Since the XES peak position of UF_4 is determined by a localized f^2 configuration, the negative comparative shift of the URu_2Si_2 spectra indicates a more fully screened core hole, which indicates more occupied $5f$ weight (not less), that is, an f^3 component to the wavefunction. These simple comparisons therefore yield one of the main conclusions of the present study: a significant, if not dominant, f^3 component to the URu_2Si_2 wavefunction exists.

In addition, the enhanced width of the URu_2Si_2 resonance may suggest an intermediate occupancy of the $5f$ orbital, either due to a partially-filled metallic $5f$ band, a Kondo-driven intermediate valence effect, or a mixture of both. Unfortunately, unlike data from $\delta\text{-Pu}^{44}$, or even

α -U,⁴³ there are no spectra collected at any of the E_i considered here that show visible indications of multiple contributions to the main XES peaks indicative of mixed valence. For a more quantitative consideration, we turn to the results from the detailed fits.

Two fit models were considered: Model #1 allows only a single configuration, while Model #2 allows for up to three configurations to exist. The fit results are summarized in Table I, together with previous results on the standard materials and α -U.⁴³ The fits are both of high quality and the results from each model are not easily discernible. The somewhat higher-quality fit uses Model #2, which is displayed in Fig. 5. While this model is significantly better than Model #1 in a statistical sense, the fits are not visibly very different, and systematic errors (especially due to the line shape) remain the main contribution to the quality-of-fit parameter (proportional to a statistical- χ^2). We therefore do not make a judgment here as to which fit model is more appropriate; in Sec. IV we discuss some reasons for favoring Model #2, although the results aren't very different. Fit methods are described in Ref. 40. In particular, the fits utilize a parametrized $\eta(\epsilon)$ where the contribution to each resonance includes a Gaussian peak and an arctan-like function (an integrated pseudo-Voigt). The energy scale E_{gi} is defined here as the excitation energy from the $2p_{3/2}$ shell into the unoccupied states associated with the f^2 configuration. The E_{if} energy scale is defined similarly. The Model #2 fits assume an intermediate valence model where the Coulomb interaction is sufficient to split the potential f^2 , f^3 , and f^4 configurations, using a fixed energy separation of 7.2 eV as determined previously.⁴³ Peak assignments (including in Model #1) are assigned relative to the main f^2 peak in UF_4 . See Table I for further details.

It is crucial to note that the results in Table I are for fits to data collected only at one temperature. Data collected at other temperatures between 10 K and 300 K look very similar, with no clear trend in n_f using the Model #2 constraints (Fig. 6). Note that there is no significant difference between the data collected in the two experimental runs, which were about one year apart, indicating that if any oxidation on the surface is affecting the measurement (that is, artificially giving too much f^2 weight), it is stable over this time scale. Taken together, we estimate $n_f = 2.87 \pm 0.08$, including possible $\pm 5\%$ systematic error in the configuration fractions.

IV. DISCUSSION

Before discussing the data and their implications for the nature of the $5f$ states in URu_2Si_2 , we need to draw the distinction between “delocalization” and “itinerancy” as they relate to the RXES technique presented here. This technique is not sensitive to whether given spectroscopic features are associated with a band that cuts across the Fermi energy and typically are described as

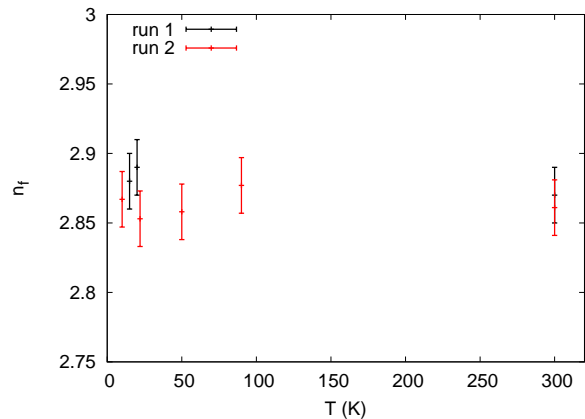


FIG. 6: Total $5f$ occupancy estimate n_f of URu_2Si_2 as a function of temperature from both experimental runs. The lowest measured temperature is 10 K. No measurable temperature dependence was observed. Taking all these data together and allowing for some systematic error gives $n_f = 2.87 \pm 0.08$.

itinerant. Rather, the technique is sensitive to, as described in Sec. I, how well these electrons screen the core hole as a consequence of the strength of their Coulomb interaction. This interaction is substantial for an orbital strongly localized to the vicinity of the core hole, such as the $4f$ orbital. A more extended, delocalized orbital, like a d orbital or a light-actinide $5f$ orbital, has a weaker interaction, and may not split the configurations in Eq. 2. The observation of a split peak is therefore a hallmark of a *localized* $5f$ orbital (which may still contribute weakly to the conduction band through hybridization and the Kondo effect), but the lack of a split peak only indicates a more extended, delocalized orbital, which may or may not contribute to the Fermi surface. We have therefore endeavored to use the word “itinerant” here only when we are discussing or comparing data to experiments indicating a Fermi surface or a model with one.

Bearing this distinction in mind, there are several useful conclusions to draw by comparing the best fit parameters from the various materials with those of URu_2Si_2 (Table I). E_{gi} , as stated above, is arbitrarily set to coincide with the f^2 peak position. Unlike in lanthanide systems (or in the limited number of plutonium systems that have been measured), E_{gi} can shift to higher energies if an orbital becomes more delocalized, and thus fails to screen the core hole as effectively. This change in screening is the reason that appropriate standard materials are so important, since the origin of a given feature could be otherwise misinterpreted. Here, we see that the three relatively localized standard materials have very similar E_{gi} s and the sharpest σ_p s, with the increased width of UO_2 likely due to crystal field splitting of the d states.³² Changes in E_{if} are linear with E_{gi} , consistent with no significant off-diagonal elements in the transition matrix in this energy range.

It is interesting to compare these data to those from

TABLE I: RXES fit results for data collected at 20 K for URu₂Si₂ and for previously published work⁴³ on UCd₁₁ and UF₄ as examples of localized f^3 and f^2 compounds, UO₂ as an example of a system with significant ligand field splitting, and α -U as an example of a metal with itinerant $5f$ electrons. E_{gi} and E_{if} are defined in these fits to correspond to the f^2 resonance position. The energy separation between each of the f^2 , f^3 , and f^4 resonances is set to $\Delta E = 7.2$ eV, as determined from the fits to the UCd₁₁ data and the UF₄ data. See Sec. II for a further description of the fit parameters. Reported errors assume normally distributed errors and are obtained from the covariance matrix. Systematic errors are likely larger for the configuration fractions, and we estimate $\pm 5\%$ as a reasonable error estimate for both the configuration fractions and n_f . Note that average result of data collected at difference temperatures and including systematic error gives $n_f = 2.87 \pm 0.08$ (see Fig. 6).

Compound	E_{gi} (eV)	E_{if} (eV)	σ_p (eV)	p/s	f^2 (%)	f^3 (%)	f^4 (%)	n_f (e ⁻) ^a
UCd ₁₁	17175.0(1)	3560.0(1)	1.9(1)	3.3(1)	13.5(7)	86(1)	0.1(5)	2.86(1)
UF ₄	17174.3(1)	3560.3(1)	1.2(4)	9	100(3)	0(2)	0(1)	2.00(3)
UO ₂	17173.9(1)	3559.8(1)	1.9(4)	5.6(2)	95(2)	5(1)	0(1)	2.05(2)
α -U	17176.9(1)	3562.5(1)	2.9(4)	1.5(1)	46(2)	54(3)	0(2)	2.54(2)
URu ₂ Si ₂ Model #1	17178.6(1)	3564.6(1)	3.4(1)	1.7(1)	0	100	0	3
URu ₂ Si ₂ Model #2	17178.1(2)	3564.0(2)	3.1(4)	2.0(1)	11(2)	89(2)	0.0(5)	2.89(2)

^aAs with other parameters, reported errors assume normally distributed errors and these fits are for data at only one temperature. Systematic errors on n_f are thought to approach 0.08. See Fig. 6.

recent results on α -U,⁴³ which should correspond to an itinerant material. The XES spectra of α -U shown in Fig. 7 are clearly even a little broader than the URu₂Si₂ spectra, displaying more indications to the eye of shoulders and other features indicative of multiple $5f$ configurations. The α -U data are, in fact, consistent with a local density of states modeled on two dominant $5f$ configurations, f^2 and f^3 , corresponding to an $n_f = 2.54 \pm 0.08$. As expected for an itinerant material, E_{gi} and E_{if} are significantly higher than for the standard materials (about 3 eV), consistent with a more delocalized $5f$ orbital.⁴³

The most informative fit parameters are those relating to the individual peak width σ_p and the relative configuration fractions. The largest peak widths here are for α -U and URu₂Si₂, and as such may be indicative of $5f$ orbital delocalization due to the distribution of possible Coulomb interactions. A similar situation is observed for Pu intermetallics, where the compounds with the lowest linear coefficient to the electronic specific heat⁴⁴ have the largest peak widths⁴⁰ (excluding PuO_{2.06} which likely has an enhanced width due to crystal field splitting of the d states).

The comparisons of the data and fit results between URu₂Si₂, α -U, and the standard materials thus strongly favor a large, delocalized f^3 component to the ground state of URu₂Si₂. In particular, the fit using Model #2 over several temperatures (Fig. 6) indicate an n_f of 2.87 ± 0.08 . Unfortunately, as noted in Sec. III, we do not judge the difference between fits with Model #1 (single f^3 configuration) and Model #2 (a mixture of f^2 , f^3 , and f^4 configurations) to be enough to support the presence of some f^2 component due to potential systematic errors, especially in the lineshape model. However, a comparison to the α -U results supports this possibility, since the value of σ_p for the Model #2 fit is nearly identical to that of the fit to α -U data where more clearly

visible evidence exists for multiple configurations. The fact that multiple excitation peaks, shoulders, or other visible evidence is not observed in the data in Fig. 7 is because URu₂Si₂ is more dominated by a single configuration than α -U. We do not categorically rule out that URu₂Si₂ has no f^2 component, however.

Taking these results together, we conclude that URu₂Si₂ is dominated by a delocalized f^3 configuration and is possibly weakly intermediate valent. Although it has a similar n_f to strongly localized UCd₁₁, the shift in E_{gi} and the enhanced peak width σ_p both indicate a delocalized $5f$ orbital.

Although $5f$ electron involvement in the conduction band is strongly supported by these data, either through a $5f$ band or a Kondo-like mechanism, it is important to note that the lack of temperature dependence in n_f is typical of other uranium intermetallics, even in those with Kondo temperatures between 100 K and 200 K, where one would expect shifts in n_f at temperatures above 20 K.⁵¹ The lack of temperature dependence here is consistent with angle-integrated photoemission results.⁵² Like the angle-integrated photoemission experiments, the RXES results presented here are sensitive to the average of all potential $5f$ configurations. We point out that if only a small portion of the Fermi surface, *eg.* the Z -point hole pocket, displayed any temperature dependence, RXES would not be very sensitive to it.

Although no temperature dependence is observed in these data from room temperature to 10 K and the measurements are consistent with a partially filled $5f$ band, it is instructive to consider the implications in light of the Anderson model.⁵³ As such, this part of the discussion is intended to be only qualitative or semi-quantitative in order to illustrate the implications of the measurements reported above. With a qualitative goal in mind, we can consider these results using the non-crossing approxima-

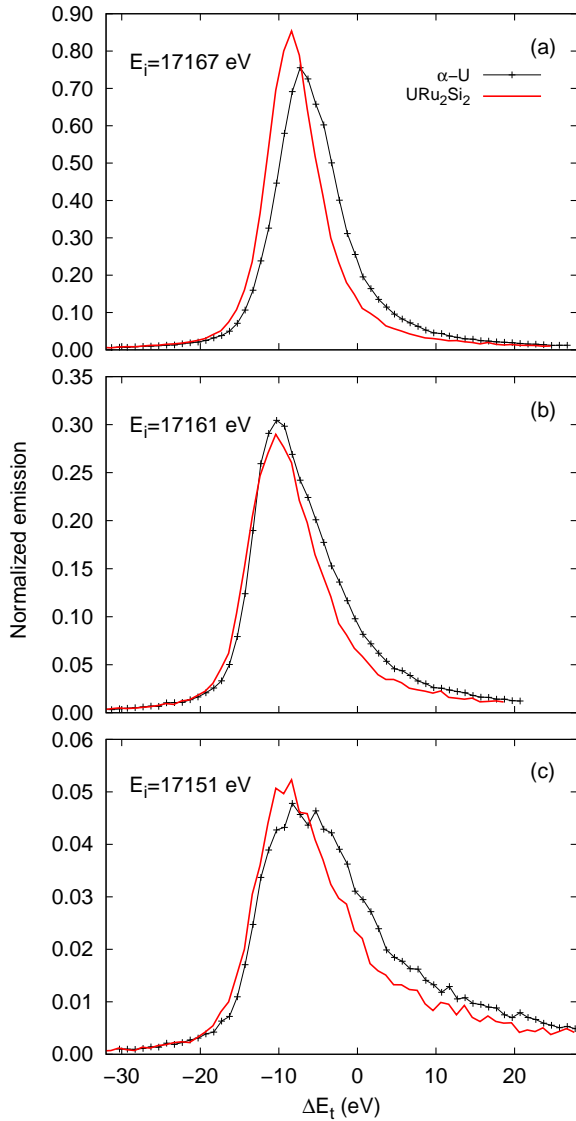


FIG. 7: Comparison of XES data at 20 K for α -U (data from Ref. 43) and URu_2Si_2 as a function of $\Delta E_t = E_t - E_{if}$ to accentuate possible differences in $5f$ occupancy. Note that these data are normalized to the peak XES data with E_t at an incident energy well above the absorption edge, in contrast to those in Fig. 4.

tion (NCA).⁵⁴ Within a simplification of this model for a single f electron (which can be taken as a single unpaired f electron), one can consider:⁵⁵

$$n_f(T) = 1 - \delta n_{\text{charge}}(T) - \delta n_{\text{spin}}(T), \quad (3)$$

where the Kondo physics affects δn_{spin} , with

$$\delta n_{\text{spin}}(0) = \frac{\pi T_{\text{nca}}}{\nu \Gamma} \left(1 + \frac{\pi T_{\text{nca}}}{\nu \Gamma} \right)^{-1}, \quad (4)$$

where ν is the magnetic degeneracy, $\Gamma = \pi \rho V^2$ is the hybridization strength, ρ is the density of electronic states

at the Fermi energy, V is the hybridization matrix element between f and the conduction electrons, and T_{nca} is the Kondo temperature as defined in the NCA formalism. $\delta n_{\text{charge}}(T)$ changes very slowly with T where $T \ll \epsilon_f$, and so we can consider the low- T value to be constant:

$$\delta n_{\text{charge}} \equiv \delta n_{\text{charge}}(0) = \frac{\Gamma}{\pi \epsilon_f}, \quad (5)$$

where ϵ_f is the absolute energy of the f level with respect to E_F . We note that

$$\lim_{T \rightarrow \infty} \delta n_{\text{spin}}(T) = 0,$$

and therefore the high-temperature limit of n_f is $\tilde{n}_f = 1 - \delta n_{\text{charge}}$.

Within this formalism, we expect to observe a total change in n_f of $\Delta n_f(0) \approx \frac{1}{2} \delta n_{\text{spin}}(0)$ from $T = 0$ K to about $T \approx T_{\text{nca}}$. Here, it is important to distinguish between the coherence temperature $T_{\text{coh}} \approx 70$ K and the estimate of the Kondo temperature $T_K \approx 370$ K.⁵⁶ For this rough discussion, taking $T_K \sim T_{\text{nca}} \sim 300$ K and including no more than $\Delta n_f(0) \lesssim 0.05$ limits the ratio of T_{nca}/Γ to about 0.3. We have confirmed this limit with a more detailed NCA calculation.⁵⁷ For smaller T_{nca} , this limit would be even more restrictive. Therefore, the main conclusion of this qualitative discussion is simply that charge fluctuations dominate the interpretation of the RXES data. We stress that this estimate is in the single-impurity regime above the coherence temperature, and definitely above the HO transition, below which Hall effect measurements indicate a very small carrier concentration of only ~ 0.05 holes per formula unit within the usual 1-band approximation. Such a low carrier concentration would not provide enough conduction holes to quench any unpaired $5f$ electron spins in any Kondo effect,⁵⁸ a situation particularly important when one moves away from a single-impurity model and toward a lattice model.⁵⁹

The picture that emerges from these data is therefore one that is dominated by conventional charge fluctuations such as one would expect from itinerant $5f$ electrons, with very little if any temperature dependence indicating strong hybridization between the $5f$ orbital and the conduction band. On the other hand, a contribution from an f^2 configuration is consistent with the RXES data. It remains possible that the delocalized f^3 -like contributions originate from the majority portion of the Fermi surface, while a minority portion, such as the Z -point hole pocket, are the source of more localized f^2 -like behavior. If this is the case, any temperature dependence in the U L_{III} -edge absorption of this minority portion would be obscured by the majority f^3 -like portion. In other words, these data are easily rectified with the itinerant f^3 band theories, but could still allow for a localized f^2 theory if that theory only applied to a small portion of the Fermi surface or some other minority portion of the electronic structure. This dichotomy is therefore suggestive of a 2-fluid like interpretation, and, in fact, 2-fluid

theories appear in many explanations of various actinide phenomena,^{60–65} including of URu₂Si₂.^{18,66}

V. CONCLUSION

RXES measurements at the U L_{III} edge and the U $L_{\alpha 1}$ emission indicate that URu₂Si₂ has a delocalized $5f$ orbital with a mean occupancy $n_f = 2.87 \pm 0.08$. The conclusion of a delocalized orbital is derived from the line shape of the RXES signal, by the shift in the L_{III} threshold energy, and the lack of temperature dependence. These results are consistent with EELS and photoemission experiments (see Sec. I). These results are not consistent with theoretical models that require a localized f^2 state to generate crystal field splitting in the $5f$ manifold, unless this state could be in the minority compared to a majority f^3 band.

Acknowledgments

CHB acknowledges several useful conversations with Jason Jeffries, Nicholas Butch, Andrew Wray, Jonathon

Denlinger, and Jon Lawrence. JGT gratefully acknowledges support during FY 2014 from the Lawrence Livermore National Laboratory (LLNL) PRT program for his sabbatical at Lawrence Berkeley National Laboratory (LBNL). Work at LBNL was supported by the Director, Office of Science, Office of Basic Energy Sciences (OBES), of the U.S. Department of Energy (DOE) under contract DE-AC02-05CH11231. LLNL is operated by Lawrence Livermore National Security, LLC, for the U.S. Department of Energy, National Nuclear Security Administration, under Contract DE-AC52-07NA27344. RXES data were collected at the Stanford Synchrotron Radiation Lightsource, a national user facility operated by Stanford University on behalf of the DOE, OBES. Work at Los Alamos National Laboratory was performed under the auspices of the U.S. DOE, OBES, Division of Materials Sciences and Engineering.

-
- * Present address: Departments of Chemistry and Physics, University of Wisconsin-Oshkosh, WI 54901, USA
- † Present address: National High Magnetic Field Laboratory, Tallahassee, FL 32310, USA
- ‡ Present address: Center for High Pressure Science & Technology Advanced Research, 1690 Cailun Rd., Bldg #6, Pudong, Shanghai 201203, P. R. China
- ¹ T. T. M. Palstra, A. A. Menovsky, J. van den Berg, A. J. Dirkmaat, P. H. Kes, G. J. Nieuwenhuys, and J. A. Mydosh, *Phys. Rev. Lett.* **55**, 2727 (1985).
- ² M. B. Maple, J. W. Chen, Y. Dalichaouch, T. Kohara, C. Rossel, M. S. Torikachvili, M. W. McElfresh, and J. D. Thompson, *Phys. Rev. Lett.* **56**, 185 (1986).
- ³ C. Broholm, J. K. Kjems, W. J. L. Buyers, P. Matthews, T. T. M. Palstra, A. A. Menovsky, and J. A. Mydosh, *Phys. Rev. Lett.* **58**, 1467 (1987).
- ⁴ See, for example, articles in *Special Issue: Hidden order in URu₂Si₂*, *Phil. Mag.* **94**, Issue 32-33, (2014).
- ⁵ J. A. Mydosh and P. M. Oppeneer, *Phil. Mag.* **94**, 3642 (2014).
- ⁶ J. A. Mydosh and P. M. Oppeneer, *Rev. Mod. Phys.* **83**, 1301 (2011).
- ⁷ P. Chandra, P. Coleman, and R. Flint, *Phys. Rev. B* **91**, 205103 (2015).
- ⁸ P. Chandra, P. Coleman, and R. Flint, *Nature* **493**, 621 (2013).
- ⁹ A. I. Tóth and G. Kotliar, *Phys. Rev. Lett.* **107**, 266405 (2011).
- ¹⁰ J.-J. Su, Y. Dubi, P. Wölfle, and A. V. Balatsky, *J. Phys.: Condens. Matter* **23**, 094214 (2011).
- ¹¹ H. Harima, K. Miyake, and J. Flouquet, *J. Phys. Soc. Jpn.* **79**, 033705 (2010).
- ¹² K. Haule and G. Kotliar, *Nat. Phys.* **5**, 796 (2009).
- ¹³ P. M. Oppeneer, J. Ruzs, S. Elgazzar, M.-T. Suzuki, T. Durakiewicz, and J. A. Mydosh, *Phys. Rev. B* **82**, 205103 (2010).
- ¹⁴ P. M. Oppeneer, S. Elgazzar, J. Ruzs, Q. Feng, T. Durakiewicz, and J. A. Mydosh, *Phys. Rev. B* **84**, 241102(R) (2011).
- ¹⁵ H.-H. Kung, R. E. Baumbach, E. D. Bauer, V. K. Thorsmølle, W.-L. Zhang, K. Haule, J. A. Mydosh, and G. Blumberg, *Science* **347**, 1339 (2015).
- ¹⁶ See Supplementary Materials for Ref. 15.
- ¹⁷ C. R. Wiebe, J. A. Janik, G. J. MacDougall, G. M. Luke, J. D. Garret, H. D. Zhou, Y.-J. Jo, L. Balicas, Y. Qiu, J. R. D. Copley, et al., *Nat. Phys.* **3**, 96 (2007).
- ¹⁸ K. R. Shirer, A. C. Shockley, A. P. Dioguardi, J. Crocker, C. H. Line, N. apRoberts Warren, D. M. Nisson, P. Klavins, J. C. Cooley, Y.-F. Yang, et al., *PNAS* **109**, E3067 (2012).
- ¹⁹ N. P. Butch, M. E. Manley, J. R. Jeffries, M. Janoschek, K. Huang, M. B. Maple, A. H. Said, B. M. Leu, and J. W. Lynn, *Phys. Rev. B* **91**, 035128 (2015).
- ²⁰ K. Behnia, R. Bel, Y. Kasahara, Y. Nakajima, H. Jin, H. Aubin, K. Izawa, Y. Matsuda, J. Floquet, Y. Haga, et al., *Phys. Rev. Lett.* **94**, 156405 (2005).
- ²¹ L. A. Wray, J. Denlinger, S.-W. Huang, H. He, N. P. Butch, M. B. Maple, Z. Hussain, and Y.-D. Chuang, *Phys. Rev. Lett.* **114**, 236401 (2015).
- ²² S. Tonegawa, K. Hashimoto, K. Ikada, Y.-H. Lin, H. Shishido, Y. Haga, T. D. Matsuda, E. Yamamoto, Y. Onuki, H. Oikeda, et al., *Phys. Rev. Lett.* **109**, 036401 (2012).
- ²³ S. Tonegawa, S. Kasahara, T. Fukuda, K. Sugimoto, N. Yasuda, Y. Tsuruhara, D. Watanabe, Y. Mizukami, Y. Haga, T. D. Matsuda, et al., *Nat. Comm.* **5**, 4188 (2014).

- ²⁴ F. Bourdarot, B. Fåk, K. Habicht, and K. Prokeš, *Phys. Rev. Lett.* **90**, 067203 (2003).
- ²⁵ A. Grauel, A. Böhm, H. Fischer, C. Geibel, R. Köhler, R. Modler, C. Schank, F. Steglich, G. Weber, T. Komatsubara, et al., *Phys. Rev. B* **46**, 5818 (1992).
- ²⁶ T. Durakiewicz, *Phil. Mag.* **94**, 3723 (2014).
- ²⁷ I. Kawasaki, S.-I. Fujimori, Y. Takeda, T. Okane, A. Yasui, Y. Saitoh, H. Yamagami, Y. Haga, E. Yamamoto, and Y. Onuki, *Phys. Rev. B* **83**, 235121 (2011).
- ²⁸ S. Fujimori, T. Ohkochi, I. Kawasaki, A. Yasui, Y. Takeda, T. Okane, Y. Saitoh, A. Fujimori, H. Yamagami, Y. Haga, et al., *J. Phys. Soc. Jpn* **81**, 014703 (2012).
- ²⁹ A. F. Santander-Syro, M. Klein, F. L. Boariu, A. Nuber, P. Lejay, and F. Reinert, *Nature Phys.* **5**, 637 (2009).
- ³⁰ J.-Q. Meng, P. M. Oppeneer, J. A. Mydosh, P. S. Riseborough, K. Gofryk, J. J. Joyce, E. D. Bauer, Y. Li, and T. Durakiewicz, *Phys. Rev. Lett.* **111**, 127002 (2013).
- ³¹ J. R. Jeffries, K. T. Moore, N. P. Butch, and M. B. Maple, *Phys. Rev. B* **82**, 033103 (2010).
- ³² J. G. Tobin, S.-W. Yu, C. H. Booth, T. Tylliszczak, D. K. Shuh, G. van der Laan, D. Sokaras, D. Nordlund, T.-C. Weng, and P. S. Bagus, *Phys. Rev. B* **92**, 035111 (2015).
- ³³ L. Tröger, D. Arvanitis, K. Baberschke, H. Michaelis, U. Grimm, and E. Zschech, *Phys. Rev. B* **46**, 3283 (1992).
- ³⁴ W. Kohn and T. K. Lee, *Phil. Mag. A* **45**, 313 (1982).
- ³⁵ J. L. Sarrao, C. D. Immer, C. L. Benton, Z. Fisk, J. M. Lawrence, D. Mandrus, and J. D. Thompson, *Phys. Rev. B* **54**, 12207 (1996).
- ³⁶ C. H. Booth, D. Kazhdan, E. Werkema, M. D. Walter, W. W. Lukens, E. D. Bauer, Y.-J. Hu, L. Maron, O. Eisenstein, M. Head-Gordon, et al., *J. Am. Chem. Soc.* **132**, 17537 (2010).
- ³⁷ P. G. Allen, J. J. Bucher, D. K. Shuh, N. M. Edelstein, and T. Reich, *Inorg. Chem.* **36**, 4676 (1997).
- ³⁸ S. D. Conradson, K. D. Abney, B. D. Begg, E. D. Brady, D. L. Clark, C. den Auwer, M. Ding, P. K. Dourhout, F. J. E. Faller, P. L. Gordon, et al., *Inorg. Chem.* **43**, 116 (2004).
- ³⁹ D. Sokaras, T. C. Weng, D. Nordlund, R. Alonso-Mori, P. Velikov, D. Wenger, A. Garachtchenko, M. George, V. Borzenets, B. Johnson, et al., *Rev. Sci. Instrum.* **84**, 053102 (2013).
- ⁴⁰ C. H. Booth, S. A. Medling, Y. Jiang, E. D. Bauer, P. H. Tobash, J. N. Mitchel, D. K. Veieers, M. A. Wall, P. G. Allen, J. J. Kas, et al., *J. Elec. Spec. Rel. Phen.* **194**, 57 (2014).
- ⁴¹ J.-P. Rueff and A. Shukla, *Rev. Mod. Phys.* **82**, 847 (2010).
- ⁴² O. Keski-Rahkonen and M. O. Krause, *Atomic Data and Nuclear Data Tables* **14**, 139 (1974).
- ⁴³ P. Soderlind, A. Landa, J. G. Tobin, P. Allen, S. Medling, C. H. Booth, E. Bauer, J. C. Cooley, D. Sokaras, T.-C. Weng, et al., *J. Electr. Spec. Rel. Phen.* **207**, 14 (2016).
- ⁴⁴ C. H. Booth, Y. Jiang, D. L. Wang, J. N. Mitchell, P. H. Tobash, E. D. Bauer, M. A. Wall, P. G. Allen, D. Sokaras, D. Nordlund, et al., *Proc. Natl. Acad. Sci. U. S. A.* **109**, 10205 (2012).
- ⁴⁵ S. L. Dudarev, D. Nguyen Manh, and A. P. Sutton, *Phil. Mag. B* **75**, 613 (1997).
- ⁴⁶ S.-W. Yu, J. G. Tobin, J. C. Crowhurst, S. Sharma, J. K. Dewhurst, P. Olalde-Velasco, W. L. Yang, and W. J. Siekhaus, *Phys. Rev. B* **83**, 165102 (2011).
- ⁴⁷ J. J. Rehr, J. J. Kas, F. D. Vila, M. P. Prange, and K. Jorissen, *Phys. Chem. Chem. Phys.* **12**, 5503 (2010).
- ⁴⁸ R. W. G. Wyckoff, *Crystal Structures* (Interscience Publishers, New York, 1964), 2nd ed.
- ⁴⁹ A. C. Larson, R. B. Roof, and D. T. Cromer, *Acta Cryst.* **17**, 555 (1964).
- ⁵⁰ T. Vitova, K. O. Kvashnina, G. Nocton, G. Sukharina, M. A. Denecke, S. M. Butorin, M. Mazzanti, R. Caciuffo, A. Soldatov, T. Behrends, et al., *Phys. Rev. B* **82**, 235118 (2010).
- ⁵¹ Although not explicitly mentioned in Ref. 44, all data reported therein were collected at temperatures of 20 or 30 K and at room temperature.
- ⁵² S. H. Yang, H. Kumigashira, T. Yokoya, A. Chainani, N. Sato, T. Komatsubara, S. J. Oh, and T. Takahashi, *J. Electron Spectrosc. Relat. Phenom.* **78**, 143 (1996).
- ⁵³ A. C. Hewson, *The Kondo Problem to Heavy Fermions* (Cambridge University Press, Cambridge, 1993).
- ⁵⁴ N. E. Bickers, D. L. Cox, and J. W. Wilkins, *Phys. Rev. B* **36**, 2036 (1987).
- ⁵⁵ D. L. Cox, Ph.D. thesis, Cornell University (1985).
- ⁵⁶ J. Schoenes, C. Schönenberger, J. J. M. Franse, and A. A. Menovsky, *Phys. Rev. B* **35**, 5375 (1987).
- ⁵⁷ J. M. Lawrence, P. S. Riseborough, C. H. Booth, J. L. Sarrao, J. D. Thompson, and R. Osborn, *Phys. Rev B* **63**, 054427 (2001).
- ⁵⁸ S. Burdin, A. Georges, and D. R. Grempel, *Phys. Rev. Lett.* **85**, 1048 (2000).
- ⁵⁹ E. D. Bauer, C. H. Booth, J. M. Lawrence, M. F. Hundley, J. L. Sarrao, J. D. Thompson, P. S. Riseborough, and T. Ebihara, *Phys. Rev. B* **69**, 125102 (2004).
- ⁶⁰ J. Schoenes, O. Vogt, J. Löhle, F. Hulliger, and K. Matenberger, *Phys. Rev. B* **53**, 14987 (1996).
- ⁶¹ G. Zwirgagl and P. Fulde, *J. Phys.:Condes. Matter* **15**, S1911 (2003).
- ⁶² F. Steglich, P. Gegenwart, R. Helfrich, C. Langhammer, P. Hellmann, L. Donnevert, C. Geibel, M. Lang, G. Sparn, W. A. and G. R. Stewart, et al., *Z. Phys. B* **103**, 235 (1997).
- ⁶³ D. L. Cox and M. Jarrell, *J. Phys.: Condens. Matter* **8**, 9825 (1996).
- ⁶⁴ S. Nakatsuji, D. Pines, and Z. Fisk, *Phys. Rev. Lett.* **92**, 016401 (2004).
- ⁶⁵ Y.-f. Yang and D. Pines, *PNAS* **109**, E3060 (2012).
- ⁶⁶ Y. Okuno and K. Miyake, *J. Phys. Soc. Jpn.* **67**, 2469 (1998).